5 October 2015

TO: Tech Note archive
FROM: William Cooper
SUBJECT: Workflow to reproduce or update the technical note

1 Purpose

This section describes the workflow for the code in "WindUncertainty.Rnw" that generates the Technical Note on “Characterization of Uncertainty in Measurements of Wind from the NSF/NCAR Gulfstream V Research Aircraft.” WindUncertainty.Rnw contains both text (in LaTeX format) and R processing script for the analysis in this Technical Note. The description of workflow provided here includes the process of collecting the observations and processing them to data files, the data archives used, the steps required to generate the plots and other results including the instances where manual intervention is required to identify appropriate subsets of the data, the relevant R code and LaTeX documents, and all the steps leading to the generation of the text in the Technical Note. "WindUncertainty.Rnw" incorporates a set of child documents containing the individual sections of the document, so the workflow of each of those child documents is also described in detail. The final authority regarding workflow is the set of ".Rnw" documents themselves, which are part of the archive, but this overview and diagrams will help explain the workflow at a general level and so should substitute for reading the R and LaTeX code in most cases. The intent is to describe the workflow in sufficient detail to support replication of the analysis and figures presented in this Technical Note, and also to enable changes based on new data or new analysis approaches.

2 Acquisition of the primary data

Most of the measurements used in this report were collected using the NSF/NCAR GV research aircraft during the DEEPWAVE project of 2014. As described in the body of the technical note, the onboard data-acquisition program ’aeros’ recorded the data in digital format, and those data files were then processed by the program ’nimbus’ to produce an archive in NetCDF format. The software management group of NCAR/EOL maintains a version-controlled archive of these programs, so if they are of interest they can be obtained by contacting the data-management group of EOL (at this or this address). The data files available from NCAR/EOL can be found at links on this URL. The details of the processing algorithms are documented here: Processing Algorithms. These procedures as they pertain to the measurement of wind are also documented in the "Introduction" to the present technical note. The resulting data files contain measurements in scientific units and brief descriptions of each measurement.

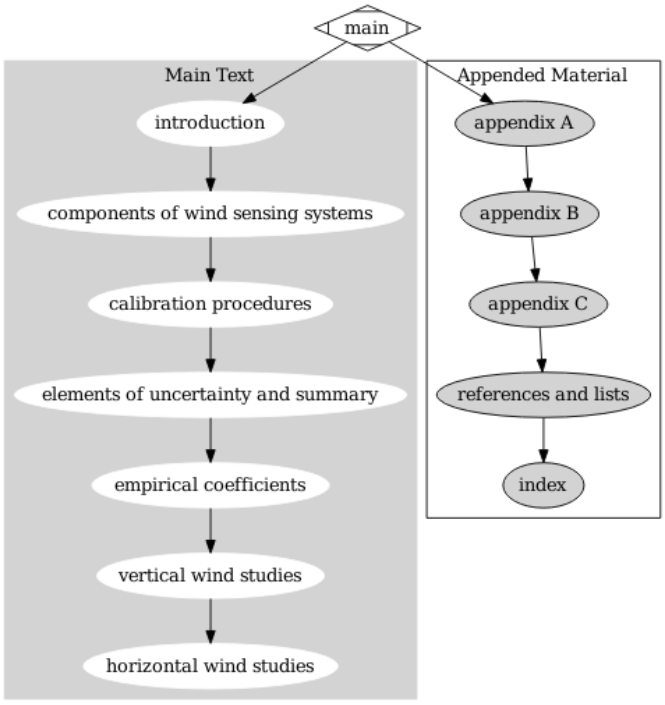

Figure 1: Top-level flow chart describing the order of processing for the main program.

3 Overview of the workflow

The Technical Note is organized into seven sections, three appendices, some lists including citations, and an index. Each of the sections in contained it a separate "child" document that is loaded during compilation and so included in the document produced by the file "WindUncertainty.Rnw". An additional document containing the pitch-correction subsection is also loaded when section 6 is processed. A top-level view of the sequence is provided by Fig. 1.

Some information on the rationale for the organization of the technical note is provided in Appendix A, where the conventions for uncertainty analysis being followed in this technical note are discussed. The central result of the uncertainty analysis is contained in Section 4 (Elements of uncertainty and summary). The sections before this one are mostly descriptions of the measuring systems in terms of component measurements and how they are calibrated and combined to obtain measurements of wind. The last three sections present key studies of the measurements used to reduce uncertainty and check the results. Section 4 relies on information presented in detail in the last three sections, but the intent is that the section be readable as a suimmary of the results, with references and links should more information be desired by the reader.

An additional appendix, Appendix B, provide some limited characterization of the ability of the systems to measure the characteristics of turbulence. Appendix C is a discussion of the attempt to facilitate reproducibility of this technical note, and the present memo describing workflow is a key

feature of that attempt.

The description of workflow provided in this memo is lacking in specifics regarding, for example, how particular parts of the data were selected for plots and how those plots were generated. However, that information can be found in detail in the code itself, and almost all steps leading to plots, fit coefficients, or other numerical results can be found in that way. The few exceptions (e.g., the variance spectra in Appendix B) are mentioned specifically and a general path to their creation is described. Because this information is so complete in the master files themselves, no effort will be made here to develop a similar provenance diagram showing these details.

Describing one additional aspect of the document structure may help readers of the code: Where the expression "Sexpr{}" exists in the LaTeX code, the quantity in braces is a reference to variables or functions in the preceding R code. This is a feature provided by the "knitr" processing, which derives from sweave and so traces back to S, the predecessor to R; hence the contraction for S-expression. In this way, results from calculations (e.g., coefficients from a linear fit) can be entered into the text with assurance that the text will represent exactly the results of the calculations. This avoids the danger of entering numerical results manually into the text, when those results might change for different data or different fit constraints.

In the next section, the workflow for each of the seven sections shown in Fig. 1 will be discussed, with additional diagrams for the details internal to each section.

4 Workflow diagrams and discussion for individual sections

4.1 Introduction

The general structure of an Rnw file like Introduction.Rnw is that R code is incorporated in "chunks" that have special delimiters and unique names, while the remainder of the content is LaTeX. Introduction.Rnw has only one chunk, the "parent-intro" chunk that provides a link to the parent file "WindUncertainty.Rnw" so that it can be compiled to PDF format by referencing the LaTeX preamble and document definitions contained in that parent file. Other sections also have a similar initial chunk, which makes construction of each section possible without requiring construction of the entire document, so working with the individual sections is faster and easier. Otherwise, the Introduction.Rnw file is all text. The "Overview" provides an initial description of the wind-sensing systems on the aircraft and some references to previous studies and source material. Section 1.2 provides the equations used to calculate wind, for all the systems, including the determination of the air motion relative to the aircraft ("relative wind") and the angle transformations required to obtain the Earth-relative wind vector from the relative wind and the aircraft orientation and motion. This material is drawn from standard sources as cited, but it is included because it provides a reference for calculations used throughout the Technical Note.

Throughout this and all other sections, there are interspersed "\index" and "\sindex" LaTeX commands that are used to compile the index, list of symbols, and list of variable names provided at the end of the document. These have been inserted manually, so they represent considerable

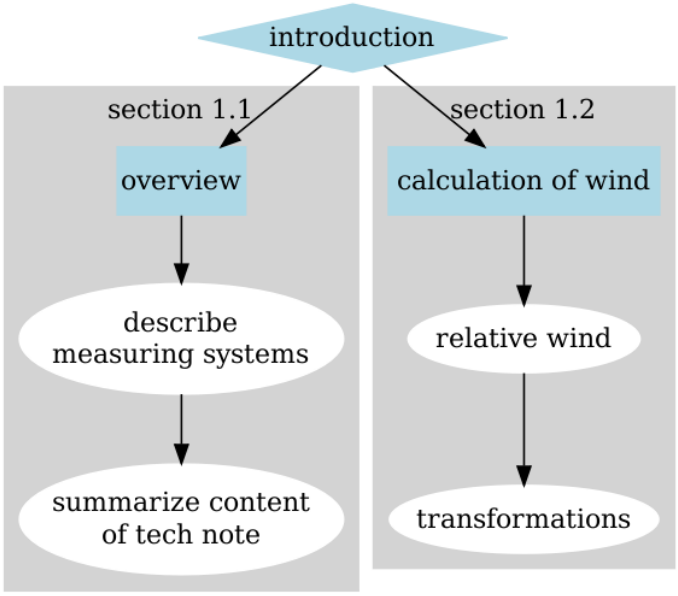

Figure 2: Workflow for Section 1 (Introduction).

work yet have led to results that are incomplete because selections for inclusion have been made subjectively and with varying care throughout the document. This is an aspect of the Technical Note that could be improved by additional work and review, so the present status is a compromise made on the basis of estimated added value vs effort required. Another aspect of the document structure that might be questioned is the frequent use of footnotes. Despite standard advice that such footnotes should be avoided where possible, they are included liberally in this document in order to document subtle aspects of the work while not distracting from the main flow of the text.

In the case of this and most other sections of the document, the initial draft was constructed using "LyX" because it provides a convenient way of generating LaTeX code while also incorporating R chunks and the results can be exported to .Rnw format. The LyX files are not included in the project archive because there has usually been significant editing after the initial files were generated so they would not represent the final product. The resulting .Rnw file was then further edited in RStudio and converted to the final text document using the "compile PDF" function in RStudio. The references and Appendix C in the Technical Note provide further information on the specific versions used and citations to authors of the packages used for R and RStudio as well as "knitr" which provides the capability of generating text documents from the Rnw files.

4.2 Components of the wind-sensing systems

Figure 3 shows the general workflow for Section 2. There are three subsections, respectively discussing the radome-based, gust-pod, and LAMS measuring systems for measuring wind.

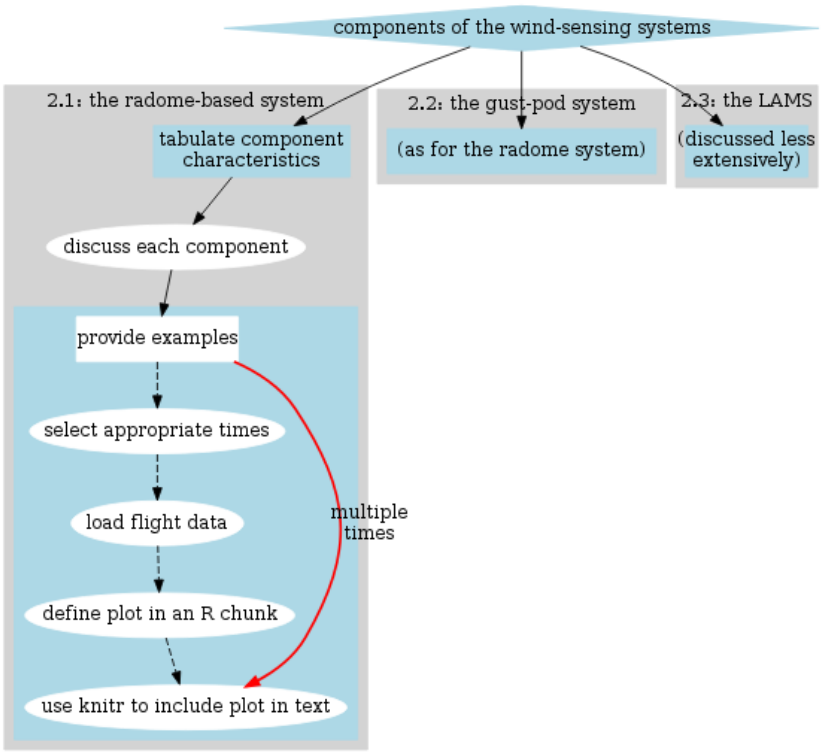

Figure 3: Workflow diagram for Section 2, generated by "ComponentsOfWindSensingSystem.Rnw".

The radome-based system

The first is the conventional system and the basis for most past measurements This is the system in most common use, so the section devotes the most space to it. Much of the information contained in these pages comes from web sites or manuals provided by manufacturers of the components or from the EOL instrument web pages, especially the section on "State Parameters". The section begins with a table (Table 1) giving instrument characteristics from these sources or occasionally from intercomparison results, and that table also includes estimates of standard uncertainties associated with the measurements. Then, for each measurement, the text includes a discussion of the component, the basis for the uncertainty estimate, and other characteristics like time response or limitations. These sections of the text then themselves serve as workflow templates for the construction of the text. References are given to documents that discuss processing algorithms or the basis for some of the estimates. In some cases (e.g., for the attitude angles measured by the inertial reference systems), comparisons between identical or similar systems are used to justify the estimates; these comparisons have been done external to this document and the results inserted manually, a violation of the general principle that the document be self-contained and self-generating. In the cases of pressure, temperature, and airspeed, a recent publication is cited because it provides more detail than it is reasonable to duplicate here and because the document is available on-line. In many cases, the specific links to the EOL instrument pages are provided where there are photographs and additional instrument characteristics for the component measurements. Some photographs of these components have been inserted into the text to show their appearance on the aircraft.

After the detailed discussion of entries in Table 1, some examples of the measurements are included to show the general nature of the measurements. The workflow diagram shows the general path taken to generate these examples, and the red arrow in the figure shows that this sequence is followed repeatedly to construct diagrams for the component measurements. For example, Fig. 3 shows the attitude angles measured by three different inertial reference systems in the course of one flight. This figure is generated by the R code in the chunk "radome-plot-angles". The following sequence can be seen in that chunk:

1. *Select appropriate times:* Flight rf16 from the DEEPWAVE project is selected, and the plot is made to cover the entire flight.

2. *Load flight data:* A set of variables is defined and then retrieved from the archived NetCDF file, and the retrieved subset is saved in a much smaller R data file that can be retrieved for subsequent runs or archived with the document. The netCDF access routine "getNetCDF()", part of the "Ranadu" package, is used for this retrieval. That package resides on https://github.com/WilliamCooper/Ranadu.git along with instructions for its use.

3. *Define plot in an R chunk:* The plot is then generated by calls in the chunk labeled "radome-plot-angles". The statements generating the plot are the calls to "plotWAC()", also part of the "Ranadu" package.

4. *Use knitr to include plot in text:* The processing program "knitr" then places the plot at an appropriate place in the text file, with caption as specified in the header of the R chunk and with sizes and locations controlled by global options set in the parent document.

This sequence is repeated for Figs. 4–7, in the respective R chunks "radome-plot-pressures", "radome-plot-airflow-angles", "radome-plot-groundspeed", and "radome-plot-wind". These all use the data retrieved for Fig. 3, so step 2 above does not need to be repeated.

The example plots could be changed easily be selecting another flight or another time period, or be selecting different variables to pass to the plotting commands.

The gust-pod system

The workflow for the gust-pod system is mostly a duplicate of that for the radome-based system, but for the component measurements for the gust-pod system (usually with variable names that include "_GP"). Table 2 provides entries similar to those in Table 1 for this system. An additional plot is generated in this section to compare the vertical wind provided by the gust-pod system to that from the radome-based system. The algorithm providing the vertical wind for the gust-pod system is newly developed in this report (Section 5), so there is extra documentation associated with it (Figs. 8–10). Like most other figures, they are generated in R chunks, respectively "vw-gp-vs-wic", "hw-gp-vs-std", and "gp-small-segment". Note that in the first of these a variable sdWICmWIG is defined as the standard deviation of the difference between the two measurements of vertical wind, and that the comparison plotted in Fig. 8 is restricted to measurements at altitudes above 25,000 ft and with roll between -5 and 5°; these were the conditions of most interest in DEEPWAVE and avoided some larger errors in the gust-pod vertical wind that arose in turns. The variable sdWICmWIG was used in a "\Sexpr{}" statement to be able to quote this result in the text. Figure 3, presented earlier in connection with the radome-based system, also included some measurements from components in the gust-pod system.

Figure 11 is another exception in the effort to make the generation of plots self-contained, because it shows the variance spectra calculated externally and inserted into this document. It was generated by a private package (called Xanadu) that is not generally available, but it uses methods documented as described in the text and as cited in earlier references. Figure 12 is also generated specially by shifting some measurements in time; the code for this shift is included in the .Rnw file but is commented and was enabled only to produce this plot, so it is another plot that is inserted into the text manually.

The LAMS

This system is still undergoing development and testing, and has been the subject of two publications references in the Technical Report, so the description included here has a different and more tentative structure. The discussion includes definition of the beam pointing angles and uncertainties associated with them, some photographs and a schematic diagram showing the system

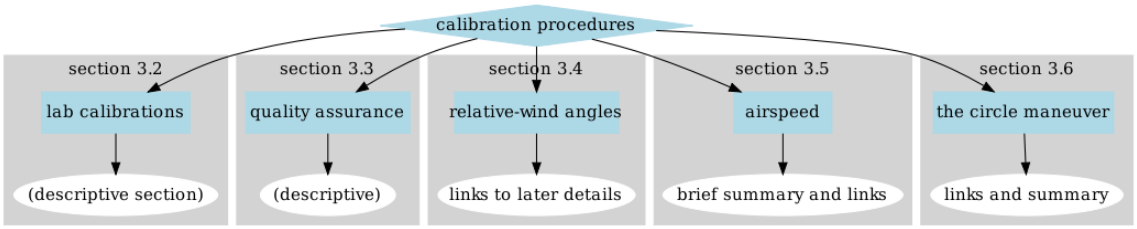

Figure 4: Workflow chart for Section 3, implemented in "CalibrationProcedures.Rnw".

(Figs. 13–16), a discussion of data-handling procedures, and some examples of measurements from the system. Figure 17 shows some sample measurements, generated in the standard way via code in R chunks "LAMS-example-1" and "transform", using data from another project and flight (HCRTEST, flight 3). The latter chunk also includes the code to transform from the aircraft reference frame (where the relative wind is defined) to the Earth-based system, following the math specified in Section 1.

4.3 Calibration procedures

The workflow for Section 3 is shown in Fig. 4. The section is mostly descriptive, so the workflow is relatively simple, consisting of describing how calibrations are performed for the component measurements of the various systems and how measurements are checked before, during, and after projects. The radome-based and gust-pod systems both rely on empirically determined functions to represent airflow angles in terms of measured pressures, so these functions are introduced here, with references to more detailed discussions to follow. This section also introduces the value of the circle maneuver when checking performance of the wind-sensing systems and refers to later discussions for the details. The reason for introducing these latter calibration procedures here is that they are used in the next section to reduce uncertainty limits for some measurements.

4.4 Elements of uncertainty and summary

Section 4 is the summary section for the Technical Note, and its conclusions are the key ones for the entire document. It serves as a summary of everything that was considered when estimating the uncertainty in wind measurements, and it provides links to other parts of the report where they justify or provide a basis for the values used in this summary. The workflow is summarized in Fig. 5. Each vertical column represents a subsection, and each will be discussed below.

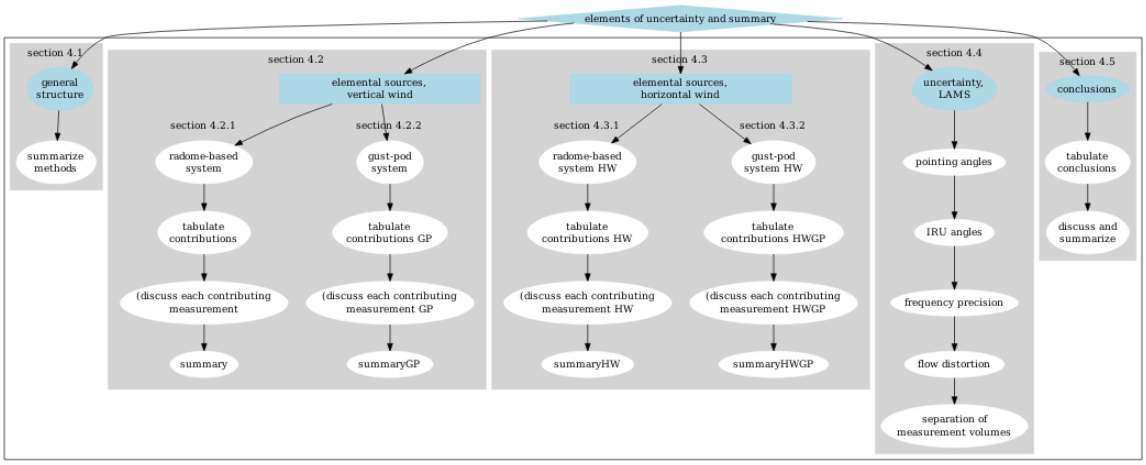

Figure 5: Workflow chart for Section 4, implemented by ElementsOfUncertaintyAndSummary.Rnw.

General structure (Section 4.1)

This is a text-only subsection without calculations. It outlines the structure to follow and calls attention to Appendix A where the structure is discussed in more detail.

Elemental sources, vertical wind (Section 4.2)

Section 4.2 contains two parallel branches, as shown in Fig. 5, one for the radome-based system and a second for the gust-pod system. Each has the same structure:

1. A summary table that lists the individual contributions to uncertainty in vertical wind at the most basic level (e.g., the transducer used to make a contributing measurement) and a estimate of the estimated limit to the bias error in that measurement, the random component of the standard uncertainty, the degrees of freedom associated with the random component, and the contribution to uncertainty in vertical wind obtained by propagating the bias limit and the standard uncertainty in the elemental source to the vertical wind through the calculation chain used for data processing. For each entry in the "bias" or "random" columns, the type of uncertainty estimate (either A or B) is also indicated; these types are discussed in Appendix A. Determining the appropriate entries in this table is the central task required to construct the analysis of uncertainty reported in this Technical Note, and substantial work is required to obtain and justify the entries in this table, as discussed in the next item. The entries in the table are defined in the R chunk labeled "table-1-elements" (for the radome system), although the table is actually Table 6. The entries are defined as R variables in this way to ensure consistency among the table entries, the discussion, and the propagated uncertainty

leading to net uncertainty in the vertical wind. For the gust pod (a new and possibly evolving system), the table entries in Table 7 are simply entered into the LaTeX table, although a better structure would duplicate that used for the radome system.

2. For each elemental source, the table entries are then discussed and justified, often with links to material elsewhere in the document including that in Tables 1 and 2 where the component measurements are listed along with specifications. In some cases (e.g., pitch) the entries included in Table 7 are substantially smaller than those in Table 1, so the discussion justifies that change. In other cases (e.g., QCF and ADIFR), the noise limit observed in variance spectra in regions of low turbulence is used to support the table entries.

3. Each branch concludes with a summary that provides the net uncertainty in vertical wind and any qualifications limiting the conditions under which that estimated uncertainty is valid. This estimate is then the primary result of the analysis in this Technical Note. The procedure used for the radome-based system is to reference the result from the R chunk "table-1-elements" where the tabular entries are added in quadrature to obtain the net uncertainty, and these results are then referenced via "\Sexpr{}" in the LaTeX text.

Elemental sources, horizontal wind (Section 4.3)

Section 4.3 is constructed following the model defined above for Section 4.2, as also shown in Fig. 5, so the discussion above applies to this section also. The only complication arising in this section is that the estimates need to be made separately for the longitudinal and lateral components of the horizontal wind, so the table entries (Tables 8 and 9) include two propagated uncertainties for these two components, and the net uncertainty then is determined for each separately.

Uncertainties associated with the LAMS (Section 4.4)

The LAMS is still under development, so the information presented here is preliminary and likely to change with new versions of the instrument. This is an all-text subsection without R code. The workflow leading to the mathematical derivations is described by including complete derivations (constructed by Matt Hayman). For the discussion of beam pointing angles, the results from section 2.3.2 are used for the estimated uncertainty in pointing angle that is then propagated to wind measurements. This is followed by a mathematical discussion of the effect of uncertainty in measurements from the inertial reference system (referencing equations in section 1), the frequency precision is estimated from instrument characteristics, and the discussion of flow distortion uses an airflow field from computational fluid dynamics modeling that was provided (as proprietary information to be used for purposes like this but not to be distributed further) by the aircraft manufacturer. This subsection concludes with a discussion of effects arising in turbulent conditions from different wind vectors being present in the different sensitive volumes of a multi-beam system, again based on theoretical arguments.

Conclusions (Section 4.5)

In this concluding summary of the results, the uncertainty estimates are presented in Table 10, which is constructed for the radome items by reference to the R variables calculated in the R chunk "table-1-elements" but for the gust-pod by manual repetition of the results presented in the earlier sections. This table is then discussed with consideration of resulting uncertainty in wind speed and wind direction, and the dominant sources of uncertainty are highlighted to guide possible efforts to improve the measurements. This section is the "Conclusions" section for the entire Technical Note.

The final component constructed in this section is a plot showing the distribution in the differences between the vertical wind as measured by the radome-based system and the gust-pod system. To construct this plot, an R data.frame was constructed in R chunk WICWIGcalc by including measurements from all DEEPWAVE research flights where the gust-pod measurements appeared valid, with a few additional periods excluded when there seemed to be problems with one of the measurements. Specifically, measurements from flights 1, 5–10, 12–14, 16, 20–22, and 26 were used, except the time period from 8:05:00 to 8:40:00 was excluded from flight 1 and the period from 9:50:00 to 10:30:00 was excluded from flight 23. Most exclusions were because the inertial system used with the gust pod seemed to have anomalously large differences vs. that used with the radome system, and a few exclusions were because icing or freezing water in the sensing lines interfered with the measurements of angle of attack from the radome. The measurements used in the plot were also restricted to flight levels above 35,000 ft and having roll in the range from -5 to 5° (to eliminate turns). The data.frame was constructed by a series of calls to Ranadu::getNetCDF()" to retrieve the variables needed. The data.frame so constructed was saved with the name Sect4WICvsWIG.Rdata, and this data.frame is included in the data archive for this Technical Note. Then the plot itself was constructed in the R chunk "WICWIGdiff", in this case using the R package ggplot2 with a specific theme (theme_WAC) provided by the "Ranadu" package. As for other plots generated in R chunks, this plot was included at an appropriate location in the text file after processing by the "knitr" package, with caption as provided in the chunk header.

4.5 Sensitivity coefficients (empirical coefficients)

Section 5 contains the work to determine sensitivity coefficients for the radome-based and gust-pod systems. The sensitivity coefficients result from linear fits that provide measurements of angle of attack and sideslip angle from the pressure differences measured on the radome or gust pod. They are determined empirically because, for the radome system, the geometry is not a simple shape that would be amenable to theoretical representation, and for the gust pod the location of the probe below the wing of the aircraft introduces significant flow-distortion effects not easily represented theoretically. To find empirical relationships that provide valid estimates of the angle of attack or sideslip angle, some basis for calibration is needed. Because when the vertical wind is zero the angle of attack can be calculated from the pitch angle, airspeed, and rate of climb, this provides the needed basis for the fits if flight segments can be used where the vertical wind is zero. Even for varying vertical wind, the fit procedure will be valid if the vertical wind averages to zero over

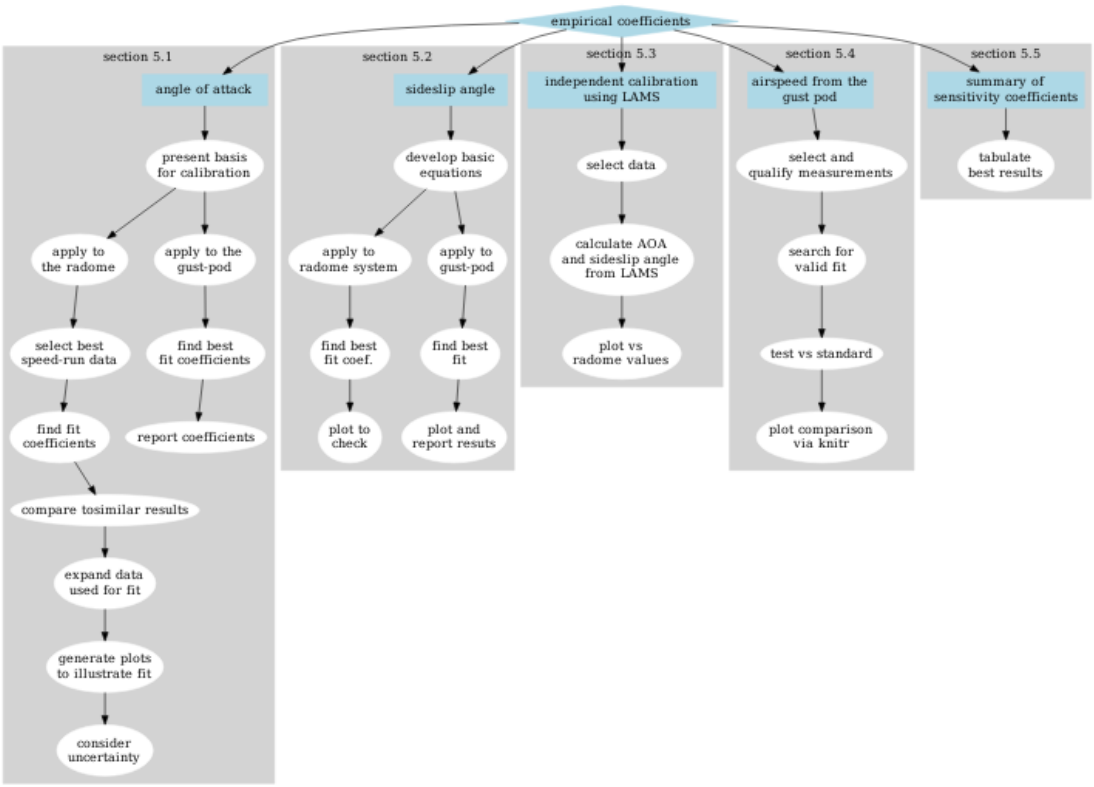

Figure 6: Workflow diagram for Section 5, produced by “SensitivityCoefficients.Rnw”.

the flight segment used (provided the fluctuations are not correlated with the pitch angle). For the sideslip angle, a similar reference can be obtained using the assumption that, when the sideslip angle is changed by the pilots, the horizontal wind should remain the same. The preferred way to obtain data to support these fits is, in the case of angle of attack, to fly level and straight "speed runs" where the airspeed is varied through the flight envelope of the aircraft, and in the case of sideslip angle to use "yaw maneuvers" in which sideslip is forced by rudder action in level flight without roll (to the extent that this is possible).

Separate empirical relationships are needed for the radome-based system and for the gust-pod system, and each system needs relationships for both airflow angles, so there are four parallel workflow branches, two each in Sections 5.1 and 5.2. The steps are similar in all, so only the case of angle-of-attack for the radome-based system will be presented in detail. Only comments about how they differ will be offered for the other three.

Angle of attack (Section 5.1) – radome-based system

1. Present the mathematics that provides a reference for the calibrations, and describe the required nature of the data to be used. The key equation is (31), and the task becomes to find a representation of α^* as given by that formula in terms of measured quantities, especially the pressure difference between top and bottom ports on the radome (called ADIFR in the netCDF variables in the data files).

2. *Select best speed-run data,* make data selections and then load the required measurements. An example is the R chuck titled "getData-AOA". This chunk includes specifications of the measurements needed and then uses Ranadu::getNetCDF() to load the data.frame. For initial calculations, four speed runs were identified by searching for level flight segments where the airspeed was varied from minimum to maximum flight speed, thus changing the angle of attack through a wide range of angles. The selected times are listed in the text. It was necessary to perform these maneuvers during the DEEPWAVE flights to have these measurements available, so the workflow in this case extended back to the flight plans used for the field project. In addition, "getData-AOA" loaded other data that were used later in the analysis to expand the data used for fits. Another subtle point in data acquisition for these fits was that an algorithm for correcting the measured pitch, developed in Section 6.4 of the Technical Note, was applied to the measurement of pitch before calculating the reference values α^* specified by (31). The justification is that it is desirable to use the best available measurements of pitch in these fits, even though the correction has not yet been presented and justified in the document. For this purpose, the routine Ranadu::CorrectPitch() was used to add a variable "PITCHC" to each retrieved data.frame, and that variable was then used to calculate the reference value α^*.

3. *Find fit coefficients.* For this step, there was a substantial amount of exploratory work not reported in the section, as various combinations of measurements were used in linear fits and tested for their ability to represent α^* as in (31).

(a) Perhaps a more systematic approach would have been better, but the guidance used was to check the standard deviation between angle of attack as generated by the empirical formula vs. α^* and judge the value of added complexity in the formula by the resulting reduction in standard deviation.

(b) The R linear-fit routine "lm" itself provides information on the significance of each term in the linear fit, so that was also helpful in deciding if it was worthwhile to keep additional terms. However, a strong preference was given to simpler formulas because a danger in this approach is that, if high-order terms are included and then conditions outside the range of parameters used in the fit subsequently occur in routine usage, extrapolation beyond the valid range of the formula can give large errors. Therefore, in cases where formulas with more terms gave a better fit, if the standard deviation decreased by less than about 10%, the simpler formula was favored.

(c) Many of the possible dependences are listed in the text. All these and others were explored in the process of constructing this section of the Technical Note.

(d) The result for the radome was that a simple linear dependence on ADIFR/QCF (the ratio of the pressure difference on the radome between bottom and top ports, normalized by the measured dynamic pressure QCF) was adequate. The next term having a significant effect was that term multiplied by the Mach number M; i.e., M ADIFR/QCR.

(e) Early in this section, in the R chunk "Initialization", a function "SummarizeFit()" was defined for printing results obtained from "lm" during fitting. This function was used to include fit results into the text, for example as listed in identifiable font with gray shading in Section 5.1.2.

(f) To check the fit results visually, a scatterplot of α as produced by the empirical formula with fit coefficients vs α^* was constructed, in R chunk "AOA-fit-and-plot", This plot appears in the text as Fig. 19, placed by "knitr" after construction using routines from the R package "ggplot2" using the custom theme "theme_WAC" provided by the package "Ranadu" and with the caption provided by the chunk header.

(g) At this point in the analysis, there were some checks to see if shifts in timing of the measurements could improve the fits. The code for this purpose is included (see R chunks "adjust-timing" and "cycle-thru-times"), but the result was that adjustments did not have a significant effect so this code is commented and suppressed during final generation of the Technical Note.

4. *Compare to similar results.* Because measurements of vertical wind are of paramount importance to the DEEPWAVE project, the selected coefficients were those providing the best representation for that project. However, the approach documented in this section has been followed using data from previous projects, and an emperical relationship has been developed that is considered "standard" and is documented in the technical note on Processing Algorithms. Therefore, Fig. 20 was constructed to show that the fit obtained for DEEPWAVE produces almost the same results as using that standard relationship. This plot is generated by R chunk "plot-comparison-to-standard".

5. *Expand the range of data used for the fit*

   (a) An expanded data set was then used to repeat the fit. The data used for that fit was selected to include altitudes up to FL450 (to be sure to span the region of interest to DEEPWAVE). Times selected are given in the text. The selections were made to include cases spanning a wider range in altitude and to include measurements later in flights (where fuel born changed to typical angle of attack), but to emphasize regions where it appeared reasonable to assume the vertical wind was zero at least in the average over short flight legs. Fit results from this data set are quoted in the text. See the R chunks "switch-to-expanded-dataset" and "get-data-all-flights-radome-aoa" as well as the earlier chunk "AOA-fit-and-plot".

   (b) A recommendation was then made to use the best coefficients determined to this point with (35) to represent angle of attack for the DEEPWAVE project, but to return to the standard coefficients as a starting point for other projects. The coefficients from the best fit are incorporated into the text vis "\Sexpr{}" commands after the coefficients were isolated from the summary returned by "lm" using the R function "coef()".

6. *Generate plots to illustrate the fits.* The remaining plot (Fig. 21) was generated in the "get-data-all-flights-radome-aoa" chunk. A comparison to the measurements from the entire project was also added and a summary of the fit results was included in the text.

7. *Consider uncertainty.*

   (a) For the next segment of the text, the uncertainty applicable to the empirical coefficients obtained in the earlier part of this subsection was discussed. The fit results from the R routine "lm" provided a full correlation matrix for the uncertainty in the fit results, which indicated that the uncertainties in the two coefficients of a fit to (33) were highly correlated with negative correlation, leading to the estimated uncertainty in angle of attack quoted in the text.

   (b) The "expanded" dataset (not the full-project dataset) was then subdivided into subsets where selections were random but exclusive, and fit coefficients were calculated from those subsets to determine the range of coefficients that would result. Different subset sizes were explored, as were different repetitions of the random selections. A subset size of 100 (or 177 measurements per subset) was selected, and the experiment (consisting of assignment of all measurements to subgroups and the calculation of fit coefficients for each subgroup) was repeated 50 times, giving 5000 values for each coefficient. The standard deviations in the coefficients so determined, reduced by an estimated number of degrees of freedom for this approach, then gave values that could be compared to the values estimated from the fit as in item (a) above, with reasonable consistency.

   (c) A comment was then added to indicate that the largest undertainty associated with these fits arises from the assumption that the vertical wind is zero when using (31) as the reference for the fit. Some arguments were offered to support that this assumption

might be reasonable, and an estimated uncertainty assigned, but this remains a critical weakness of the approach. In the future, this might be helped by the analysis of more measurements from other projects.

Angle of attack (Section 5.1) – gust-pod system

The primary differences in workflow for the gust-pod system vs. that for the radome-based system are that the development is less extensive (because the system is new and not crucial to most science applications) and, because the gust-pod is located under the wing in a region of disturbed airflow, a more elaborate empirical formula turned out to be required for a good representation of the reference values from (31). After substantial but unsystematic exploration of possibilities, (36) was selected as the least complicated choice that could provide an acceptable standard deviation between the results and the calibration values. A figure (Fig. 22) similar to Fig. 19 was generated, following the model used for Fig. 19, to illustrate the results, and the summary of the fit is included in the text for this case and also for the all-project results.

Sideslip angle (Section 5.2) – radome-based system and gust-pod system

For sideslip, the reference value β^* given by (38) arises instead from the assumption that the horizontal wind remains steady through yaw maneuvers so changes in heading, corrected for any changes in the vector difference between groundspeed and wind during the maneuver, will provide a reference sideslip for calibration. The workflow is a straightforward adaptation of that for angle of attack:

1. *Select appropriate data periods for the fit, and acquire the data.* This step requires that appropriate maneuvers be flown during the research project, in this case DEEPWAVE, and that the times for the maneuver be found manually and entered into the processing program, just as for angle of attack.

2. *Find best fit and plot:* In the case of sideslip, a simple linear dependence on the pressure difference measured by the horizontally separated ports on the radome or the gust pod was adequate. Fit coefficients and a plot are included for the radome-based and gust-pod systems, and listings documenting the fit results are included in the text.

Independent calibration using LAMS (Section 5.3)

The LAMS was not operational during DEEPWAVE, the project used for most of this report, but a comparison between LAMS measurements and those from the radome-based system was possible using the subsequent flights in the "HCRTEST" program. Appropriate data were loaded as part of the section provided by "ComponentsOfWindSensingSystem.Rnw", so that saved data.frame was loaded from the saved file (DataFrameL.Rdata") for reuse here. The line-of-sight airspeed

measurements from the LAMS were transformed to wind measurements in the R chunk "LAMS-transform", with appropriate geometry for this project as specified by the angles "Theta" and "Phi" in that chunk. Because beam-2 was forward in that project, the wind calculations had to be based on three beams with beams 1 and 3 off-axis but beam 2 forward, a special configuration. In addition to normal wind calculations (following the approach of Section 1b of the Technical Note), the measurements were also used to calculate the angle of attack and the sideslip angle solely from the LAMS measurements. These provided independent measurements that could be compared to the results using the empirical coefficients and equations of the preceding subsections. The comparisons were made as follows:

1. A suitable data segment that included a good speed run (judged to be good because of the relative constant values of horizontal and vertical wind) was selected and specified in the text.

2. The fit procedure described in the subsection "Angle of attack (Section 5.1) – radome-based system", item 3, was repeated using the LAMS-measured angle of attack as the reference for the fit instead of (31). The resulting slope of the fit was then compared to that obtained previously. (Comparing the constant term in the fit was not meaningful because the orientation of the LAMS was offset from the longitudinal axis of the aircraft, leading to an expected difference in the first term in the fit coefficients.)

3. In addition, the angle of attack determined in the standard way was compared to that determined from the LAMS measurements by constructing a scatterplot of the two measurements, as shown in Fig. 25. That figure was generated in the R chunk "LAMS-attack-plot" using the R package ggplot2.

4. This was then repeated for sideslip, except that the results are discussed only in terms of the fit results and no plot was included.

True airspeed from the gust-pod system (Section 5.4)

The goal of this subsection is to obtain an empirical relationship for the airspeed that references only the measurements made by the gust-pod system, so that the two systems might provide independent measurements of the wind. (The gust-pod system does not measure temperature or humidity, both of which enter the calculation of airspeed, so that dependence still is shared between the two systems.) This goal proved difficult to achieve because the gust-pod is in a location where there is significant airflow distortion, and as a result all the measurements including those of static and dynamic pressure are affected. The approach taken was to argue that, for the conventional radome-based system, the airspeed is a function only of q/p, the ratio of dynamic to static pressure, temperature, and (to a small degree) humidity, so if the gust-pod measurements can be used in an empirical formula that gives q/p then an airspeed can be measured that does not rely on the standard measurements of pressure.

These were the workflow steps:

1. Select appropriate measurements and load them into an R data.frame. Describe the selections made in the text and document the restrictions imposed on the data to avoid problematic regions (like turns or low-level flight).

2. Explore fits using equations with various measurements and ratios of measurements that might be good candidates for representing the desired pressure ratio q/p in terms of measurements from the gust pod. For reference, q/p as measured by the radome-based system was used. It was found that it was difficult to find a simple relationship, but one involving 8 terms and coefficients (including a constant-offset coefficient) gave an acceptable fit.

3. The characteristics of this fit (e.g., standard deviation between the result of the empirical formula and the reference measurements) were then presented and discussed in the text, and the formula leading to airspeed from q/p was cited and used to estimate the resulting uncertainty in airspeed.

4. Two plots, Fig. 26 and 27, were then generated to compare, respectively, the pressure ratio and the airspeed obtained from the gust pod as a function of the reference value from the radome-based system. These were generated in the R chunks "plot-qp-fit" and "TAS-from-the-gust-pod-2" using standard R plot routines.

Summary of sensitivity coefficients (Section 5.5)

Section 5 concludes with a summary of the results obtained in the preceding subsections. Because the key results are scattered throughout the section, it was thought useful to repeat them in one summary. The summary is LaTeX with references via "knitr" "\Sexpr{}" statements to earlier results, to ensure consistence between this summary and the earlier statements of results. The summary also specifies the appropriate equation for which to use the specified coefficients.

4.6 Studies of the vertical wind (Section 6)

After an overview that states the intent and content of this section, there are three subsections, with workflow as indicated by Fig. 7:

The vertical velocity of the aircraft (Section 6.2)

These steps were used to construct this subsection:

1. the available measurements of rate of climb of the aircraft were discussed and presented in a table.

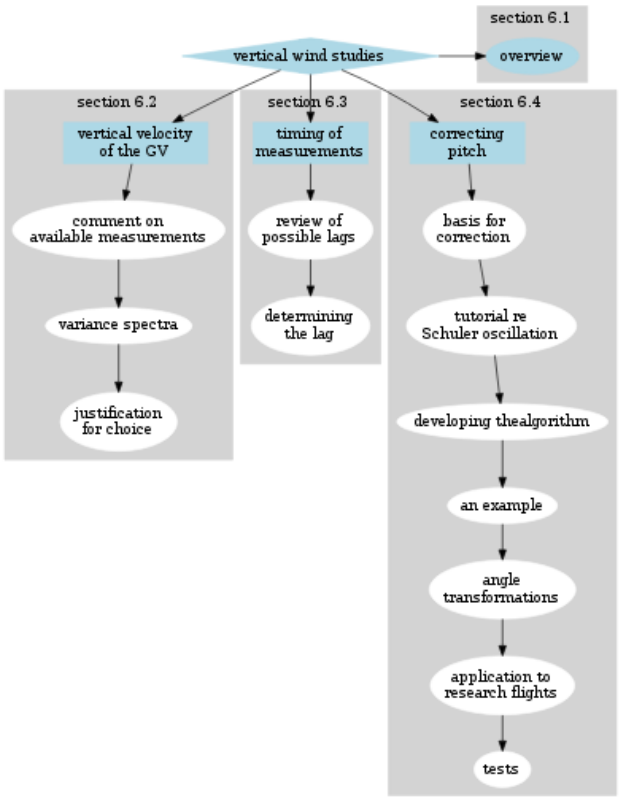

Figure 7: Workflow chart for Section 6, as incorporated in “VerticalWindStudies.Rnw”.

2. Some variance spectra were constructed for these measurements to illustrate their characteristics (Fig. 28). That figure includes variance spectra for the primary calculated vertical wind (WIC) as well as for two candidate measurements of rate of climb (GGVSPD and VSPD), as well as the relative-wind contribution (plotted as GUSTW). Like all the variance spectra in this technical note, these were constructed using the analysis program "Xanadu", which uses the "all-poles" or "maximum entropy" method of Press et al., as listed in the references. The construction of this plot showing many different variance spectra was somewhat complex; it consisted of using the python-generated code from Xanadu for each spectrum but editing the generating routine to combine all the measurements into a single python-generated plot. The plot, archived as "SpecialGraphics/VSPDspectraDW16.pdf", was generated by the python routine MEMPlotVSPD.py which referenced the temporary data files DXDAT16WIC, DXDAT16WI, DXDAT16GUSTW, DXDAT16GGVSPD, and DXDAT16VSPD. These files were all generated by individual processing in Xanadu, and the resulting python files were edited by combining the plotting segments into one file. All these files and the underlying Xanadu routine are archived in the Technical Note archive, with the exception of the core spectra analysis routine that is part of the proprietary Numerical Recipes in C package. The final plot was included in the LaTeX file using an "\includegraphics{}" statement and an associated "\caption{}" statement. The text description was then generated based on the features of this plot.

3. On the basis of these results, arguments were presented that favor use of a particular choice (GGVSPD) for rate-of-climb to be used when calculating the vertical wind, and hence a particular variable (WIC) for vertical wind.

For reference elsewhere in the Technical Note, an additional plot was generated that shows the variance spectrum for the vertical wind and separately its gust and rate-of-climb components for a region with very low turbulence. This plot (Fig. 29) was generated in ways analogous to those described in item 2 above. The discussion of this figure highlights tha noise level evident at high frequency and argues that this indicates a minimum level of turbulence that can be measured with the radome-based wind system because of random errors in measurements of the radome-port pressure and the dynamic pressure. An additional plot, Fig. 30, was constructed from a segment of the data used for the previous figure. This plot illustrates a basic flight mode of the aircraft and the generation of regular aircraft motions that must be removed for proper operation of the wind sensing system. This figure is generated in the R chunk "phugoid-plot".

Timing of measurements (Section 6.3)

This section contains studies of the possible delays among component measurements affecting the vertical wind.

1. First information on lags used in processing is reviewed for the key measurements, in an itemized list. This information regarding processing is gleaned from the netCDF data files,

which include information on time lags as variable attributes. Some information here is also quoted from instrument specifications obtained from the manufacturers.

2. Pitch maneuvers, during which the angle-of-attack and pitch are varied to induce a porpoising motion of the aircraft with period of 20 s or so, were then used to evaluate possible lags still present in the measurements. The approach taken was to search for the lags that gave the smallest variance in measured vertical wind during the pitch maneuver, because any delay among component measurements like angle of attack, pitch, and rate of climb would result in sinusoidal components in the measured vertical wind. Code for testing various shifts in included in the "VerticalWindStudies.Rnw" file but is not used in a standard run; instead, special runs were made to find the best lags, and that result is quoted in the text.

A plot showing the measured vertical wind during a pitch maneuver was then constructed (Fig. 31) to show that the best lag indeed effectively removes the imposed aircraft motion and results in measurements showing only small residual effects from the large imposed motions. That plot is generated by R chunk "plot-shifted-vertical-wind", where the data selection for the plot is also specified.

Correcting pitch for the Schuler oscillation (Section 6.4)

To generate this subsection of the report, a separate child document called "SchulerSection.Rnw" is included by an R-chunk reference in the report, via a chunk named "E3" in "VerticalWindStudies.Rnw". This section includes these steps:

1. A brief *discussion of the Schuler oscillation* and how measuring the error in Earth-relative velocity components from an inertial reference unit by comparison to GPS can lead to a correction for the error in the measurement of pitch.

2. A *tutorial section* that illustrates the nature of the Schuler oscillation, with diagrams that are generated by the R chunk "plot-illustrating-pitch-coupling" and equations developed to relate the errors in pitch and roll to the errors in groundspeed components.

3. Justification for *the correction algorithm.* The key to the algorithm is presented in equations (51) and (52).

4. An example with plots of the error components is then constructed using one of the DEEP-WAVE ferry flights, selected because the heading was steady and southbound so angle transformations do not play a significant role in the results. The errors in groundspeed components are plotted in Fig. 33, generated by the R chunk "v-errors-straight-leg" using plot routines from the "Ranadu" package and with data provided by the "reinitialization" chunk where variables and the data source are specified. The data.frame resulting from the "reinitialization" chunk is saved as "SchulerData1.Rdata" in the "DataFrames" directory, which is included in the project archive. In this section, the specific method used for determining the

errors in pitch and roll, restated as in (53) and (54), is to use Savitzky-Golay polynomials fitted to the errors in groundspeed components to determine the derivatives of those errors over a running-average period of 1013 s, a period selected to be small enough to show changes occurring even within one Schuler-oscillation period. The correction procedure for this case (without mixing of pitch and roll angles as required if the heading changes) is implemented in the R chunk "sg-poly-smoothing", and that chunk also contains the code for generating Fig. 34 showing the deduced errors in pitch and roll for this flight.

5. Because in the general case the heading does not stay constant, transformations from the Earth-based local reference frame (with east-north-up coordinates) to the aircraft body frame with axes defined by the attitude angles of the aircraft (heading, pitch, and roll). The required rotation matrix is developed in this section, using rotation matrices that are the same as those in the "Introduction" section of the Technical Note except applied in reverse order. In this way, the error components determined via (53) and (54) can be transformed to give the error components applicable to the measurements of pitch and roll in the appropriate reference frame relative to the aircraft. Because this gives the estimated error, the correction to be applied to the pitch is the negative of that estimated error. The correction procedure as described in the text was also coded into the R chunk "processing-2". The R package "signal" was used to determine the Savitzky-Golay smoothing and differentiation, after interpolation was included from the "zoo" package to deal with some missing values in the measurements. This procedure was also included in the Ranadu::CorrectPitch() function, which has been used elsewhere in this Technical Report to improve the measurements of pitch.

6. *An application to research flights* is then shown in which there are frequent changes in heading and the errors in pitch and roll are significantly larger than in the first example. Figure 35 shows the errors in groundspeed components, and Fig. 36 shows the resulting errors in pitch and roll. These are generated in the R chunks "processing-1" and "processing-2" using data selected in the first chunk and the Ranadu plot routines "plotWAC()" and "lineWAC()", which in turn use standard base R plotting calls.

7. Finally, two *tests of the pitch-correction algorithm"* are presented. For the first, flight periods were compiled in which the aircraft reversed course in level flight. A pitch error present in such a maneuver should change sign when the flight direction reverses, leading to a change in the measured vertical wind. To be able to detect such a change, regions were sought with relatively low turbulence and steady vertical wind in the two legs before and after the course-reversal turn. A table of these flight segments was generated, and the average vertical wind measurements in the straight-and-level segments preceding and following the turn were then compared in Fig. 37, generated in R chunk "reverse-course-w-comparison" to show the improvement resulting from the pitch-correction algorithm. For the second test, mean values of the vertical wind are compiled for all research flights in the DEEPWAVE project, excluding only three with measurement problems. The mean values were calculated in the R chunk "mean-vertical-wind-by-flight", where the netCDF files were read and the averages calculated with and without pitch correction. Table 11 was then generated by "knitr::Sexpr()" references to those calculated mean values, as were the summary mean values then quoted

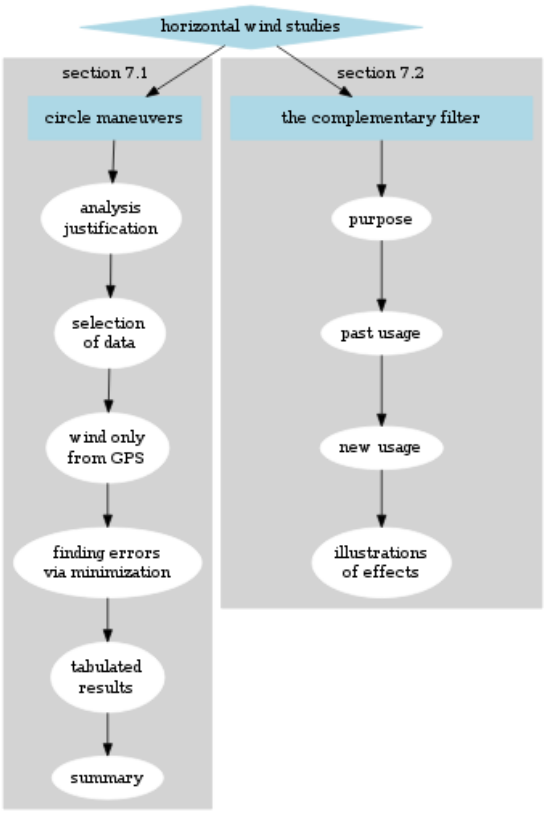

Figure 8: Workflow chart for Section 7 of the Technical Note, as generated by "HorizontalWind-Studies.Rnw".

in the text. A small improvement resulted from the pitch correction, but perhaps more significant was the calculation of the standard deviation of the change in the vertical wind produced by the pitch-correction algorithm, which was calculated in the preceding R chunk and quoted in the text via an "Sexpr{ }" function.

4.7 Studies of the horizontal wind (Section 7)

The general workflow for Section 7 is shown in Fig. 8. There are two subsections, dealing with circle maneuvers and with the complementary filter used to combine the measurements of aircraft ground speed from the inertial reference system and those from GPS.

The circle maneuvers (Section 7.1)

This section begins with a discussion of how the circle patterns were flown in the DEEPWAVE project and of the uses that can be made of these maneuvers. Figure_38 was generated to show an

example. The measurements were specified in the R chunk "getData" using a special high-rate (25-Hz) file constructed to include only the variables and times needed, and the resulting data.frame was saved in the "DataFrameCircles" for archival with the data files for this Technical Note. The plots, generated in the R chunk "circle-tracks", used "Ranadu::plotTrack()" to generate the two parts of the plot. The "drifting" plot was generated using an option in the "plotTrack()" routine that generates a "dead-reckoning" plot with the flight track corrected for the drift caused by the wind. The text specifies the time segments and flight used. These were selected because the selected flight featured circle and other maneuvers flown to assist in study of the wind measurements, so generation of the data used began during flight planning for the experiment and the times of the various maneuvers were recorded during operations.

The workflow for Section 7.1, after generation of the illustrative plot, included these steps:

1. *Justification for the analysis.* Arguments were offered to explain what is expected to be learned from the circle maneuvers and why they serve to constrain the errors entering wind calculations. This step includes development of the equations used in the analysis (59–61) and the reasons to expect that errors in airspeed and heading can be determined from fits of those equations to measurements from the circle maneuvers. Figure 39 was generated by simulation (in R chunk "sine-plot") to show the expected variation in measured wind speed for specified errors in airspeed or heading and how they can be determined from the measurements.

2. *Selection of data.* The different circle maneuvers are listed in the text, and the data are loaded into a data.frame as specified in "getData", as explained above.

3. *Finding the wind from the GPS ground track.* Measurements from a circle maneuver flown in constant-wind conditions with steady roll can be fitted using the equations developed in step 1 to find the wind without any reference to any meeasurements from the aircraft data system except the GPS ground-speed components. The results from fitting to the first circle maneuver are tabulated in Table 12, which was generated in R chunk "fitGSRMS". Two functions are defined in that chunk for use when fitting: "csq()" to provide the chi-square function for fitting, and "fitGS()" to call the R fitting routine "stats::nlm()". In addition, the routine "GSfit.R" was loaded via a "source" statement from the "chunks" directory. This performed the fit and saved the results in R variables that were then included in the table via "Sexpr{}" references. A discussion of the table was constructed to highlight features in it and summarize implications for errors and uncertainties in the measurements. Because assumptions made in processing, like the assumed heading lag, affect the results, a listing of attributes in the original netCDF data file was included in the text via the R chunk "list-THDG-attributes" and the function "Ranadu::getAttributes()". The process was then repeated for two additional circle patterns, for which Tables 13 and 14 were generated as described above for Table 12.

4. *Minimizing the variation in measured wind speed.* Next, fits of (61) to the measurements are used to determine possible corrections to airspeed and heading that will minimize variation in the wind speed around the circles. The R chunk "circle-fit-results", which included execution of the "chunks/fitCircle.R" script via a "source" reference, generated the fit coefficients.

5. *Tabulated results.* Tables 15–17 were generated by "\Sexpr{}" references to the fit results from the previous step. In addition, plots of the mean measurements of wind speed around the circles were generated as Figs. 40–42, in R chunks "first-circles", "second-circles" and "third-circles". Preceding these plots are a number of R chunks that were remnants from early stages of the analysis and are no longer used. They are suppressed by the tag "eval=FALSE" in the headers, but are kept here are a reference of some steps that were explored but not incorporated in the final document.

6. *Offset in sideslip angle.* The preceding analyses attributed the error defined as $\delta\psi'$ to the heading, but an offset in sideslip also contributes to this error. This section therefore determines the error in sideslip separately so that can be subtracted from $\delta\psi'$ to isolate the error in heading. Figures 43 and 44 were generated (in R chunks "plotSS" and "sideslip-error-histogram") using the equations developed in the text. This result indicated that a change should be made to the sideslip sensitivity coefficient determined in Section 5, so there is a forward reference to this result in that section. The mean error in Fig. 44 is then used to correct the deduced error in heading also, and the associated uncertainties in these corrections are discussed.

7. *Summary.* Because the key results are scattered through this section, a summary was constructed at the end of the section to repeat and discuss the key conclusions.

The complementary filter (Section 7.2)

The complementary filter is use for wind processing is discussed in this section, and some minor changes are proposed. The workflow steps are these:

1. *Discuss the purpose of the filter and how it has been used in past projects.* This is an all-text discussion that reviews the purpose and history of the filter.

2. *Recommended changes.* The reasons for recommending changes, including the improved performance of GPS receivers and the discovery of an error in the filter in use, are reviewed. As part of that review, a plot showing the variance spectra for the measurements to which the complementary filter is applied is shown in Fig. 45, and the coherence between the two signals in shown in Fig. 46. In addition, Fig. 47 shows the transmission of the filter previously used and the new one, which highlights the need for a change. The code includes an R equivalent of the filter used previously as well as an R representation that can be used as a replacement. The figures provide justification for the selected cutoff frequency for the new filter. The response functions are generated in R chunk "CF-response". The step concludes with recommendations for the replacement filter to be used for future projects.

5 Workflow for the appended material

5.1 Appendix A and Appendix C

These two appendices are mostly text representing supplementary material, and the workflow is evident from the text so detailed descriptions will not be induded here.

5.2 Appendix B

The description of the ability of the wind-sensing systems to measure turbulent fluctuations and characterize the turbulent energy spectrum is ancillary to the report, and the workflow is relatively similar to other sections of the Technical Note, so only a few comments are included here to highlight special features of the workflow.

1. Because the spectral analysis routine that relies on the "Xanadu" analysis package, external to R and knitr, is used often in this appendix, some special steps were used in this section. The high-rate measurements (at 25 Hz) were loaded to R data.frames from specially generated netCDF files, generated with the standard RAF processor "nimbus", and then those data.frames were written via the function "Ranadu::makeNetCDF()" to new temporary files in netCDF format that could be used by "Xanadu". A function "setXanadu()" was constructed to set the default specifications for Xanadu runs (like the start and end times and the axis limits for plots), and then system calles were used to run Xanadu to generate the variance spectra. These were renamed after return from the system call and then incorporated into the text via normal LaTeX "\includegraphics{}" calls. The plots are also saved in the "SpecialGraphics" subdirectory for archival with the Technical Note.

2. Some special analysis to characterize the effect of pressure lines was performed by Don Lenschow using other analysis tools and the plots were incorporated into the text without inclusion of the processing code.

3. The lists of symbols and variables were generated by inclusion of LaTeX commands like "\sindex[var]{...}" and "\sindex[lis]{...}", inserted manually in the text. The lists are then generated by the LaTeX command "printindex[lis]{}" and "printindex[var]{}". The index is generated similarly by including "\index{}" commands and using :printindex[idx]{}".

4. "bibtex" is used for the references.

– End of Memo –